PHYSICS OF FLUIDS **30**, 103604 (2018)

End loss for Stokes flow through a slippery circular pore in a barrier of finite thickness

Chiu-On Ng[a)] and Wenxiong Xie
Department of Mechanical Engineering, The University of Hong Kong, Pokfulam Road, Hong Kong, China

(Received 7 August 2018; accepted 13 October 2018; published online 30 October 2018)

An analytical model based on the fluid cylinder approximation and eigenfunction expansions is developed for Stokes flow through a slippery circular pore in a barrier of finite thickness. The hydraulic resistance, which comprises the end resistance and Poiseuille resistance, is determined as a function of the pore thickness, slip length of the pore wall, and proximity of pores. The results are presented to reveal how wall slip may change, quantitatively and qualitatively, the effect of the pore thickness on the end resistance. It is shown, in particular, that the use of Sampson's formula may underestimate the end loss under the effect of wall slip. Velocity slip on the wall will cause a greater departure of the velocity profile at the inlet from that of the fully developed flow, and therefore, a longer entrance length is required for the flow to attain its final state. Empirical formulas are proposed to facilitate quick calculation of the end resistance as a function of the controlling parameters. *Published by AIP Publishing.* https://doi.org/10.1063/1.5051216

I. INTRODUCTION

End loss refers to the pressure loss associated with the sudden contraction and expansion of the flow sectional area as fluid enters/exits a channel from/to a large reservoir. In high-Reynolds-number flow, the end loss is mainly due to energy dissipation by eddies in the flow separation and is therefore scaled by the velocity head. In low-Reynolds-number flow, the local pressure drop is to overcome the sharp increase in the viscous stress brought about by the sudden change in geometry, and in the absence of nonlinear inertia, the loss is linearly proportional to the flow rate. It is a common understanding that, in a sufficiently long channel, the end loss may only account for a minor fraction of the total loss. The dominant loss is usually the so-called friction loss or the pressure drop that arises because of the need to balance the skin friction on the wall. This common understanding is true when the flow has to satisfy the no-slip boundary condition, for which the flow will be sheared the most near the wall. Friction loss for a fully developed pressure-driven flow in a channel is also known as Poiseuille resistance.

For flow in micro- or nano-channels, the end loss may no longer be a minor fraction of the total loss when the channel wall is slippery. Velocity slip can significantly lower the wall friction, and hence, it is possible that the pressure drop at the inlet/outlet outweighs the pressure drop inside a low-friction channel.[1] Sisan and Lichter[2] reexamined some experimental measurements of flow rate in channels of various lengths. They showed that end effects can be appreciable in low-friction channels, such as carbon nanotubes or aquaporins. They remarked that all treatments of nanochannel flow must take into account the end effects, which will provide a finite amount of flow resistance, and therefore impose an upper bound on the flow rate even when the channel is perfectly frictionless. More recently, Belin *et al.*[3] further investigated how to reduce the end effects by modifying the shape of the entrance for a frictionless nanochannel. Ng and Sun[4] studied, using an analytical model, how pressure loss may be incurred in channel flow at a sudden change in the boundary condition from being no-slip to partial-slip.

The classical expression provided by Sampson[5] was used by Sisan and Lichter[2] to calculate the pressure drop due to the end effects. Sampson's formula is in theory only applicable to Stokes flow through a single orifice in a thin plate. Although some researchers[6,7] have proposed and confirmed the accuracy to use Sampson's formula to evaluate the end resistance for flow through a no-slip channel of finite length, the application of this formula to a slippery channel is still subject to scrutiny.

Jensen *et al.*[8] used the linear combination of the Sampson and Poiseuille resistance, which they called the Weissberg-Sampson-Poiseuille approximation, to estimate the hydraulic resistance of micro-filters. In their study, they also considered the influence of slip, which is pertinent to gas flow through microfilters. The Knudsen number for such flow is in the order of 10^{-2}, which falls into the slip-flow regime. When Jensen *et al.*[8] examined the effect of wall slip, they remarked that Sampson's solution remains valid even under slip and therefore the wall slip only affects the Poiseuille resistance. On arriving at this conclusion, they have, however, overlooked the effect of wall slip on the flow in the vicinity of the inlet to a pore. In fact, how the wall slip may affect the end loss for flow entering a slippery channel cannot be evaluated by revisiting Sampson's original theory. To this date, the use of Sampson's formula for the end resistance to flow through a channel with a slippery wall has remained a postulate yet to be tested for its accuracy. This has motivated the present study.

In this study, we shall develop a semi-analytical model for Stokes flow through distributed circular pores in a barrier

a)Author to whom correspondence should be addressed: cong@hku.hk.

of finite thickness. The primary objective is to determine how the end resistance may be affected by the wall slip. We shall show that the slip can result in an end loss that is some 20% higher than that predicted by Sampson's formula. The higher end loss caused by wall slip can be understood by looking into how flow develops in the entrance region. By comparing cases with the no-slip and partial-slip wall, we shall show that the flow has to undergo a more dramatic change in terms of kinematics and dynamics in the entrance region in the latter than in the former. We shall also propose empirical formulas that can be used for quick calculation of the end resistance as a function of the slip length, thickness of the pore, and proximity parameter.

Our problem is described in further detail in Sec. II, which contains the mathematical formulation and the expressions for the solutions. Following Wang[9] and Ng and Wang,[10] we shall develop a semi-analytical model using the methods of domain decomposition and eigenfunction expansions. The limiting case of a thin-plate orifice can be solved by the method of point match in order to satisfy mixed boundary conditions on the plate. The results and discussion are then presented in Sec. III. We shall present the results to show how the end resistance may vary depending on the pore thickness, the slip length, and the radius of the fluid cylinder representing the proximity of pores in the barrier. In the no-slip case, the end loss is virtually unaffected by the pore thickness as long as the thickness is not infinitesimally small and approaches a value slightly lower than Sampson's value as the proximity parameter becomes large. These features no longer hold in the case of the partial-slip wall. Under wall slip, the end loss is in general not close to Sampson's value, and the difference can be as much as 20%, depending on the proximity parameter and thickness of the pore.

II. PROBLEM FORMULATION AND SOLUTION

As shown in Fig. 1(a), our problem is to consider Stokes flow through a barrier of finite thickness $2l$ with distributed circular pores of radius a, where each pore has a slippery wall of partial slip length λ. When $\lambda = 0$, our problem reduces to that of Wang.[9] Following Wang,[9] we adopt the fluid-cylinder approximation[11] to define the exterior domain that encloses fluid flowing toward a particular pore; see Fig. 1(b). When the pores are positioned in a regular array, the exterior fluid domain can be represented by a polygonal cylinder, where each side of the polygon is a surface of symmetry. The polygonal cylinder is then approximated into a circular cylinder of the same cross-sectional area. For a square array (Fig. 1) where the adjacent pores are separated by a distance L, the radius of the equivalent fluid cylinder is given by $R = L/\sqrt{\pi}$. Being in direct proportion to the distance between the centers of adjacent pores L, the radius of the fluid cylinder R reflects the proximity of neighboring pores in the barrier. A pore in a barrier of finite thickness is also referred to as a hole or a channel in our discussion below. When the thickness is vanishingly small ($l \to 0$), the pore is then referred to as a thin orifice.

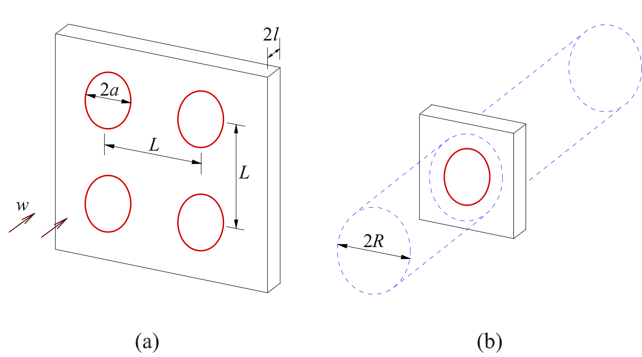

FIG. 1. (a) Flow through a barrier with pores in a regular array. (b) Fluid cylinder approximation.

The problem is formulated in terms of the primitive variables: the radial and axial velocity components (u, w) and the pressure p. Assuming axisymmetry, the flow is a function of the radial and axial coordinates (r, z) only. Figure 2 shows a longitudinal sectional view of the domains for flow toward and through a hole. Region I, the exterior domain, is a fluid circular cylinder bounded by a no-shear surface at $r = R$. Region II, the interior domain, is a circular channel of length $2l$ and is bounded by a slippery wall at $r = a < R$. Two axial coordinates, z_1 and z_2, are used to describe flow in regions I and II, respectively. It is assumed that far upstream from the hole, the pressure is zero and at the middle of region II, the pressure has dropped to $-\Delta p < 0$.

Let us introduce the following normalized variables (distinguished by an overhead caret):

$$\left(\hat{r}, \hat{z}, \hat{R}, \hat{l}, \hat{\lambda}\right) = (r, z, R, l, \lambda)/a, \quad (\hat{u}, \hat{w}) = (u, w)/U, \quad \hat{p} = p/\Delta P, \tag{1}$$

where $U = a\Delta p/\mu$ is the velocity scale, in which μ is the dynamic viscosity of the fluid. In terms of these normalized variables, the governing equations read as follows. The continuity equation is

$$\frac{1}{\hat{r}}\frac{\partial(\hat{r}\hat{u})}{\partial \hat{r}} + \frac{\partial \hat{w}}{\partial \hat{z}} = 0, \tag{2}$$

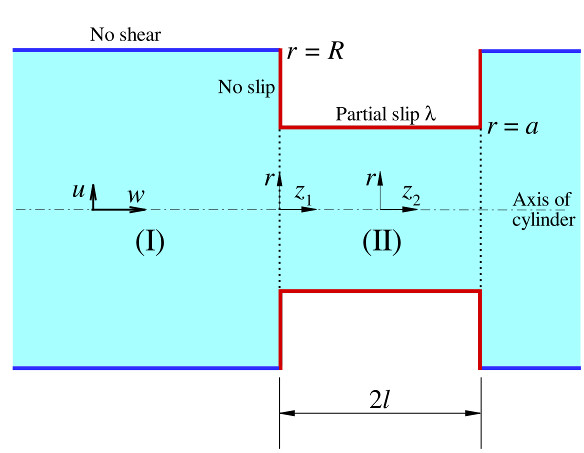

FIG. 2. Definition sketch of the problem: flow from region I into region II, representing a circular fluid-cylinder and a circular hole in a barrier, respectively. Axial coordinates z_1 and z_2 are used for the expression of solutions in regions I and II, respectively.

while the radial and axial momentum equations are

$$\frac{\partial}{\partial \hat{r}}\left(\frac{1}{\hat{r}}\frac{\partial(\hat{r}\hat{u})}{\partial \hat{r}}\right)+\frac{\partial^2 \hat{u}}{\partial \hat{z}^2}=\frac{\partial \hat{p}}{\partial \hat{r}}, \tag{3}$$

$$\frac{1}{\hat{r}}\frac{\partial}{\partial \hat{r}}\left(\hat{r}\frac{\partial \hat{w}}{\partial \hat{r}}\right)+\frac{\partial^2 \hat{w}}{\partial \hat{z}^2}=\frac{\partial \hat{p}}{\partial \hat{z}}. \tag{4}$$

These equations are subject to the following boundary conditions:

$$\hat{u}=0,\quad \hat{w}=\text{constant},\quad \hat{p}=0 \qquad \text{as } \hat{z}_1 \to -\infty, \tag{5}$$

$$\hat{u}=0,\quad \frac{\partial \hat{w}}{\partial \hat{r}}=0 \qquad \text{on } \hat{r}=\hat{R},\ -\infty<\hat{z}_1<0, \tag{6}$$

$$\hat{u}=0,\quad \hat{w}=0 \qquad \text{on } 1<\hat{r}<\hat{R},\ \hat{z}_1=0, \tag{7}$$

$$\hat{u}=0,\quad \hat{w}=-\hat{\lambda}\frac{\partial \hat{w}}{\partial \hat{r}} \qquad \text{on } \hat{r}=1,\ -\hat{l}<\hat{z}_2<\hat{l}. \tag{8}$$

From here onward, unless stated otherwise, only non-dimensional quantities are used. Hence, let us omit the carets for simplicity in what follows. The solutions presented below are similar in form to those deduced by Ng and Wang,[10] who studied Stokes flow through a periodically grooved tube.

In region I ($0<r<R, -\infty<z_1<0$), the general solutions satisfying Eqs. (2)–(4) and the boundary conditions (5) and (6) are as follows:

$$u_{\rm I}(r,z_1)=-\sum_{n=1}^{\infty}J_1(\alpha_n r)\left[(A_n+B_n)e^{\alpha_n z_1}+B_n\alpha_n z_1 e^{\alpha_n z_1}\right], \tag{9}$$

$$w_{\rm I}(r,z_1)=A_0+\sum_{n=1}^{\infty}J_0(\alpha_n r)\left[A_n e^{\alpha_n z_1}+B_n\alpha_n z_1 e^{\alpha_n z_1}\right], \tag{10}$$

$$p_{\rm I}(r,z_1)=2\sum_{n=1}^{\infty}J_0(\alpha_n r)B_n\alpha_n e^{\alpha_n z_1}, \tag{11}$$

where $A_{0,1,\ldots}$ and $B_{1,2,\ldots}$ are the undetermined coefficients, J_ν is the Bessel function of the first kind of order ν, and $\alpha_n R$ is the nth positive zero of J_1. Owing to the no-shear bounding surface, friction loss is zero in region I. Therefore, the section-mean pressure is zero as well throughout region I.

In region II ($0<r<1, -l<z_2<l$), the general solutions satisfying Eqs. (2)–(4) and the condition of zero radial velocity on the wall are as follows:

$$\begin{aligned}u_{\rm II}(r,z_2)=&\sum_{n=1}^{\infty}\frac{\sin(\beta_n z_2)}{I_0(\beta_n)}C_n\left[I_1(\beta_n r)-r\frac{I_1(\beta_n)}{I_0(\beta_n)}I_0(\beta_n r)\right]\\&-\sum_{n=1}^{\infty}\frac{J_1(\gamma_n r)}{\cosh(\gamma_n l)}[(D_n+E_n)\sinh(\gamma_n z_2)\\&+E_n\gamma_n z_2\cosh(\gamma_n z_2)],\end{aligned} \tag{12}$$

$$\begin{aligned}w_{\rm II}(r,z_2)=&\frac{P_0}{4}\left(1-r^2+2\lambda\right)+C_0+\sum_{n=1}^{\infty}\frac{\cos(\beta_n z_2)}{I_0(\beta_n)}C_n\\&\times\left\{\left[1-\frac{2I_1(\beta_n)}{\beta_n I_0(\beta_n)}\right]I_0(\beta_n r)-r\frac{I_1(\beta_n)}{I_0(\beta_n)}I_1(\beta_n r)\right\}\\&+\sum_{n=1}^{\infty}\frac{J_0(\gamma_n r)}{\cosh(\gamma_n l)}[D_n\cosh(\gamma_n z_2)\\&+E_n\gamma_n z_2\sinh(\gamma_n z_2)],\end{aligned} \tag{13}$$

$$\begin{aligned}p_{\rm II}(r,z_2)=&-1-P_0 z_2-2\sum_{n=1}^{\infty}\frac{\sin(\beta_n z_2)}{I_0^2(\beta_n)}C_n I_1(\beta_n)I_0(\beta_n r)\\&+2\sum_{n=1}^{\infty}\frac{J_0(\gamma_n r)}{\cosh(\gamma_n l)}E_n\gamma_n\sinh(\gamma_n z_2),\end{aligned} \tag{14}$$

where P_0, $C_{0,1,\ldots}$, $D_{1,2,\ldots}$, and $E_{1,2\ldots}$ are the undetermined coefficients, I_ν is the modified Bessel function of the first kind of order ν, $\beta_n=n\pi/l$, and γ_n is the nth positive zero of J_1. Note that $p_{\rm II}=-1$ at $z_2=0$, and P_0 is the Poiseuille pressure gradient in region II. Also note that $\gamma_n=\alpha_n R$.

The coefficients in the above solutions can be determined by making use of the remaining boundary conditions and matching conditions on the interface between the two regions. To this end, let us truncate A_n, B_n each to M terms, C_n to N terms, and D_n, E_n each to P terms.

In region II, the axial velocity is to satisfy the partial-slip condition at the wall,

$$w_{\rm II}=-\lambda\frac{\partial w_{\rm II}}{\partial r} \qquad \text{at } r=1. \tag{15}$$

Integrating this equation with respect to z_2 from $-l$ to l, we get

$$C_0+\sum_{n=1}^{P}(\gamma_n l)^{-1}J_0(\gamma_n)\{\tanh(\gamma_n l)D_n+[\gamma_n l-\tanh(\gamma_n l)]E_n\}=0. \tag{16}$$

On multiplying Eq. (15) by $\cos(\beta_m z_2)$, followed by integrating from $-l$ to l, we get

$$\begin{aligned}&l\left[1-\frac{2}{\beta_m}\frac{I_1(\beta_m)}{I_0(\beta_m)}-(1+2\lambda)\frac{I_1^2(\beta_m)}{I_0^2(\beta_m)}\right]C_m\\&+\sum_{n=1}^{P}J_0(\gamma_n)\left[I_{mn}^{(1)}D_n+I_{mn}^{(2)}E_n\right]=0 \quad (m=1,\ldots,N),\end{aligned} \tag{17}$$

where

$$I_{mn}^{(1)}=(-1)^m 2(\gamma_n^2+\beta_m^2)^{-1}\gamma_n\tanh(\gamma_n l), \tag{18}$$

$$\begin{aligned}I_{mn}^{(2)}=&(-1)^m 2(\gamma_n^2+\beta_m^2)^{-1}\gamma_n\\&\times\left[\gamma_n l-(\gamma_n^2+\beta_m^2)^{-1}(\gamma_n^2-\beta_m^2)\tanh(\gamma_n l)\right].\end{aligned} \tag{19}$$

On the interface between the two regions ($z_1=0$ or $z_2=-l$), the following matching conditions need to be satisfied:

$$w_{\rm I}=\begin{cases}0 & \text{on } 1<r<R\\ w_{\rm II} & \text{on } 0<r<1\end{cases}, \tag{20}$$

$$u_{\rm I}=\begin{cases}0 & \text{on } 1<r<R\\ u_{\rm II} & \text{on } 0<r<1\end{cases}, \tag{21}$$

$$\frac{\partial u_{\rm I}}{\partial z_1}=\frac{\partial u_{\rm II}}{\partial z_2} \qquad \text{on } 0<r<1, \tag{22}$$

$$p_{\rm I}=p_{\rm II} \qquad \text{on } 0<r<1. \tag{23}$$

Integrating Eq. (20) in the following manners, we get

$$\int_0^R r w_{\rm I}\,\mathrm{d}r=\int_0^1 r w_{\rm II}\,\mathrm{d}r \Rightarrow A_0=\frac{(1+4\lambda)P_0}{8R^2}+\frac{C_0}{R^2} \tag{24}$$

and

$$\int_0^R r w_{\mathrm{I}} J_0(\alpha_m r)\mathrm{d}r = \int_0^1 r w_{\mathrm{II}} J_0(\alpha_m r)\mathrm{d}r$$

$$\Rightarrow \left[\frac{J_0(\alpha_m)}{2\alpha_m^2} - \left(\frac{1}{\alpha_m^2} + \frac{\lambda}{2}\right)\frac{J_1(\alpha_m)}{\alpha_m}\right]P_0 - \frac{J_1(\alpha_m)}{\alpha_m}C_0$$
$$+ \frac{1}{2}R^2 J_0^2(\alpha_m R)A_m$$
$$- \sum_{n=1}^{N}(-1)^n\left\{\left[1 - \frac{2}{\beta_n}\frac{I_1(\beta_n)}{I_0(\beta_n)}\right]I_{mn}^{(3)} - \frac{I_1(\beta_n)}{I_0(\beta_n)}I_{mn}^{(4)}\right\}C_n$$
$$- \sum_{n=1}^{P} I_{mn}^{(5)}[D_n + \gamma_n l \tanh(\gamma_n l)E_n] = 0$$
$$(m = 1, \ldots, M), \tag{25}$$

where

$$I_{mn}^{(3)} = \left[\left(\alpha_m^2 + \beta_n^2\right)I_0(\beta_n)\right]^{-1}[\beta_n J_0(\alpha_m)I_1(\beta_n) + \alpha_m J_1(\alpha_m)I_0(\beta_n)], \tag{26}$$

$$I_{mn}^{(4)} = [I_0(\beta_n)]^{-1}\int_0^1 r^2 J_0(\alpha_m r)I_1(\beta_n r)\mathrm{d}r, \tag{27}$$

$$I_{mn}^{(5)} = \begin{cases} \left(\alpha_m^2 - \gamma_n^2\right)^{-1}\alpha_m J_1(\alpha_m)J_0(\gamma_n) & \text{if } \alpha_m \neq \gamma_n \\ \frac{1}{2}J_0^2(\gamma_n) & \text{if } \alpha_m = \gamma_n \end{cases}. \tag{28}$$

The integral in $I_{mn}^{(4)}$ is to be evaluated numerically.

Multiplying Eq. (21) by $rJ_1(\alpha_m r)$, followed by integration with respect to r as below, we get

$$\int_0^R r u_{\mathrm{I}} J_1(\alpha_m r)\mathrm{d}r$$
$$= \int_0^1 r u_{\mathrm{II}} J_1(\alpha_m r)\mathrm{d}r \Rightarrow \frac{1}{2}R^2 J_0^2(\alpha_m R)(A_m + B_m)$$
$$+ \sum_{n=1}^{P} I_{mn}^{(6)}[\tanh(\gamma_n l)(D_n + E_n) + \gamma_n l E_n] = 0$$
$$(m = 1, \ldots, M), \tag{29}$$

where

$$I_{mn}^{(6)} = \begin{cases} \left(\alpha_m^2 - \gamma_n^2\right)^{-1}\gamma_n J_1(\alpha_m)J_0(\gamma_n) & \text{if } \alpha_m \neq \gamma_n \\ J_0^2(\gamma_n)/2 & \text{if } \alpha_m = \gamma_n \end{cases}. \tag{30}$$

Multiplying Eq. (22) by $rJ_1(\gamma_m r)$, followed by integration with respect to r as below, we get

$$\int_0^1 r\frac{\partial u_{\mathrm{I}}}{\partial z_1}J_1(\gamma_m r)\mathrm{d}r$$
$$= \int_0^1 r\frac{\partial u_{\mathrm{II}}}{\partial z_2}J_1(\gamma_m r)\mathrm{d}r \Rightarrow -\sum_{n=1}^{M} I_{nm}^{(6)}\alpha_n(A_n + 2B_n)$$
$$- \sum_{n=1}^{N}(-1)^n\beta_n\left[I_{mn}^{(7)} - \frac{I_1(\beta_n)}{I_0(\beta_n)}I_{mn}^{(8)}\right]C_n$$
$$+ \frac{1}{2}J_0^2(\gamma_m)\left[\gamma_m(D_m + 2E_m) + \gamma_m^2 l \tanh(\gamma_m l)E_m\right] = 0$$
$$(m = 1, \ldots, P), \tag{31}$$

where

$$I_{mn}^{(7)} = \left[\left(\gamma_m^2 + \beta_n^2\right)I_0(\beta_n)\right]^{-1}\gamma_m J_2(\gamma_m)I_1(\beta_n), \tag{32}$$

$$I_{mn}^{(8)} = [I_0(\beta_n)]^{-1}\int_0^1 r^2 J_1(\gamma_m r)I_0(\beta_n r)\mathrm{d}r. \tag{33}$$

The integral in $I_{mn}^{(8)}$ is to be evaluated numerically.

Finally, on integrating Eq. (23) in the following manners, we get

$$\int_0^1 r p_{\mathrm{I}}\mathrm{d}r = \int_0^1 r p_{\mathrm{II}}\mathrm{d}r \Rightarrow lP_0 - 4\sum_{n=1}^{M} J_1(\alpha_n)B_n = 1 \tag{34}$$

and

$$\int_0^1 r p_{\mathrm{I}} J_0(\gamma_m r)\mathrm{d}r$$
$$= \int_0^1 r p_{\mathrm{II}} J_0(\gamma_m r)\mathrm{d}r \Rightarrow 2\sum_{n=1}^{M} I_{nm}^{(5)}\alpha_n B_n$$
$$+ J_0^2(\gamma_m)\gamma_m \tanh(\gamma_m l)E_m = 0 \qquad (m = 1, \ldots, P). \tag{35}$$

Equations (16), (17), (25), (29), (31), (34), and (35) form a system of $2 + 2M + N + 2P$ linear equations for the same number of unknowns: $P_0, C_0, A_{1,\ldots,M}, B_{1,\ldots,M}, C_{1,\ldots,N}, D_{1,\ldots,P}$, and $E_{1,\ldots,P}$. The system of equations can be solved with a standard routine. The coefficient A_0, which is the far-upstream axial velocity in region I, is then found from Eq. (24). Multiplying A_0 by the sectional area, we get the flow-rate through the hole,

$$Q = \pi R^2 A_0 = \pi\left[\frac{(1 + 4\lambda)P_0}{8} + C_0\right]. \tag{36}$$

A. Limiting case: *l* = 0

When the length l of region II tends to zero, the problem reduces to flow through a thin orifice. The boundary conditions to be satisfied at $z_1 = 0$ are

$$u_{\mathrm{I}} = 0 \qquad \text{on } 0 < r < R, \tag{37}$$

$$w_{\mathrm{I}} = 0 \qquad \text{on } 1 < r < R, \tag{38}$$

$$p_{\mathrm{I}} = -1 \qquad \text{on } 0 < r < 1. \tag{39}$$

Equations (9) and (37) imply that $B_n = -A_n$. Hence, from Eqs. (10) and (38), we get

$$A_0 + \sum_{n=1}^{M} J_0(\alpha_n r)A_n = 0 \qquad \text{on } 1 < r < R, \tag{40}$$

and from Eqs. (11) and (39), we get

$$2\sum_{n=1}^{M} J_0(\alpha_n r)\alpha_n A_n = 1 \qquad \text{on } 0 < r < 1. \tag{41}$$

The $M + 1$ unknowns, $A_{1,\ldots,M}$ and A_0, can now be determined by the method of point match. A system of equations is established when the conditions (40) and (41) are imposed at equidistant $M + 1$ discrete points in the domain $0 \leq r \leq R$. Again, the system of equations can be solved by a standard routine. The volume flow rate through the orifice is then given by $Q = \pi R^2 A_0$.

III. RESULTS AND DISCUSSION

A. Flow resistance

The hydraulic resistance of the barrier can be defined to be the pressure loss incurred by unit flow rate through the barrier. In the present problem, the pressure drop at the middle of the hole is Δp, and therefore by symmetry, the total pressure drop (i.e., the difference of the far upstream and downstream pressures) is $2\Delta p$. In terms of dimensional quantities, the flow resistance can be defined as $\varepsilon_{\mathrm{T}} \equiv 2a^3\Delta p/\mu\tilde{Q}$, or in terms of non-dimensional flow rate ($Q = \tilde{Q}/a^2U$),

$$\varepsilon_{\mathrm{T}} \equiv 2/Q. \tag{42}$$

As a common practice, we may decompose the flow resistance into the end resistance and the Poiseuille resistance,

$$\varepsilon_{\mathrm{T}} = \varepsilon_{\mathrm{E}} + \varepsilon_{\mathrm{P}}. \tag{43}$$

The end resistance ε_{E} is the loss arising from viscous effects near the entrance and exit of a channel, while the Poiseuille resistance ε_{P} accounts for the friction loss for fully developed Poiseuille flow through a channel. The end resistance, or the sum of entry and exit losses, is known to be associated with the sharp curving of streamlines as fluid particles enter/exit the channel from/to a large reservoir. The Poiseuille resistance is the part of loss occurring along the channel and is linearly proportional to the length of the channel. Note that in the present problem, the friction loss in the fluid cylinder is zero since it is bounded by a no-shear surface. We only need to consider friction loss in the circular hole in the barrier. For fully developed flow in a channel of length ℓ and with partial slip λ on the wall, the pressure loss per unit flow rate is given by

$$\varepsilon_{\mathrm{P}} = \frac{8\ell}{\pi(1+4\lambda)}, \tag{44}$$

where the channel length $\ell = 2l$ in the present problem. From these equations, we may determine the end resistance by subtracting the Poiseuille resistance from the total resistance,

$$\varepsilon_{\mathrm{E}} = \varepsilon_{\mathrm{T}} - \varepsilon_{\mathrm{P}} = \frac{2}{Q} - \frac{16l}{\pi(1+4\lambda)}. \tag{45}$$

In the limiting case of flow through a single hole in a barrier of zero thickness, corresponding to $l \to 0$ and $R \to \infty$, the flow resistance has a classical value of 3, which was first obtained by Roscoe[12] but was attributable to the earlier work by Sampson.[5] Weissberg[6] proposed that, even for a barrier of finite thickness, the Sampson value of 3 could still be used for the end resistance. Hence, in terms of the present notation, Weissberg's proposed formula reads

$$\varepsilon_{\mathrm{T}} \approx 3 + \frac{8\ell}{\pi}, \tag{46}$$

where no-slip on the wall is assumed. Dagan *et al.*[7] compared this approximation with their exact solution and found that the difference was very small, the error being less than 1%. For multiple holes, Wang[9] further introduced a proximity factor into the formula to account for the proximity of holes in the barrier. Equation (46) was called the Weissberg-Sampson-Poiseuille approximation by Jensen *et al.*,[8] who took it further to extrapolate this approximation to cover the case of flow through slippery pores. They considered that the effect of slip was only on the Poiseuille resistance and hypothesized that, in terms of the present notation,

$$\varepsilon_{\mathrm{T}} \approx 3 + \frac{8\ell}{\pi(1+4\lambda)} \tag{47}$$

would work if there is a velocity slip on the solid surface. Sisan and Lichter[2] also used a similar equation to estimate the total pressure loss for flow through a nanochannel with the end losses and boundary slip taken into account.

To this date, Eq. (47) remains an untested approximation, and it is yet to be scrutinized for its accuracy. It is a legitimate question to ask if the end resistance is still very close to the Sampson value of 3 under the influence of slip. We shall provide an answer to this question by looking into, using the present model, how the flow resistance may actually depend on the controlling parameters, including the channel length l, the slip length λ, and the radius of the fluid cylinder (also known as the proximity parameter) R.

In Fig. 3, we show ε_{T} and ε_{E}, which are computed using Eqs. (42) and (45), as functions of R and l, for $\lambda = 0$ and 100. As has been remarked earlier, our model reduces to that of Wang[9] when $\lambda = 0$. As shown in Fig. 3(a), our results (solid lines) for $\lambda = 0$ indeed agree very well with those (squares) obtained by Wang.[9] Our results also approach the asymptotic values (dashed lines) given by Dagan *et al.*[7] as $R \to \infty$. For the case $l = 0$, we also compare our results with the approximate formula put forward by Jensen *et al.*,[8] which in the present notation reads

$$\varepsilon_{\mathrm{T}} \approx 3\left(1 - 1.9\pi^{-3/2}R^{-3}\right). \tag{48}$$

The good agreement between the present and previous results serves to support the accuracy of the present model.

Figure 3(b) shows the so-called proximity effect on the end resistance, like Fig. 5 of the work of Wang.[9] Essentially, for any $l = O(1)$, all the values fall onto one single curve, and hence, the proximity effect is independent of the channel length as long as the length is not vanishingly small. This accords with the finding by Wang.[9] However, when $l = 0$ (thin orifice), the values will deviate from this common curve as R increases. Clearly, as R increases, ε_{E} will tend to the Sampson limit of 3 when $l = 0$, but a limit slightly lower than 3 when $l \sim 1$. Our results suggest that, for no-slip boundary, the channel length does have some effect on the end resistance, but such an effect is very small and is limited to very short channel length. This is consistent with what has been known in the literature: when $R \gg 1$ and $\lambda = 0$, the end resistance ε_{E} is very close to the Sampson value of 3, irrespective of the channel length. Our model generates the values of $\varepsilon_{\mathrm{E}} = 2.94$ and 2.98 at $R = 5$, for $l \sim 1$ and $l = 0$, respectively. We have here provided further evidence to support that Eq. (46) is a good approximation formula to calculate the resistance to flow through a non-slippery circular hole.

The counterparts of Figs. 3(a) and 3(b), but for $\lambda = 100$, are shown in Figs. 3(c) and 3(d). This large slip length corresponds to practically frictionless channels. It is remarkable to find that the boundary slip is to dramatically change the effect of the channel length on the end resistance. First, for different $0 \le l \le O(1)$, the values no longer fall onto a single curve.

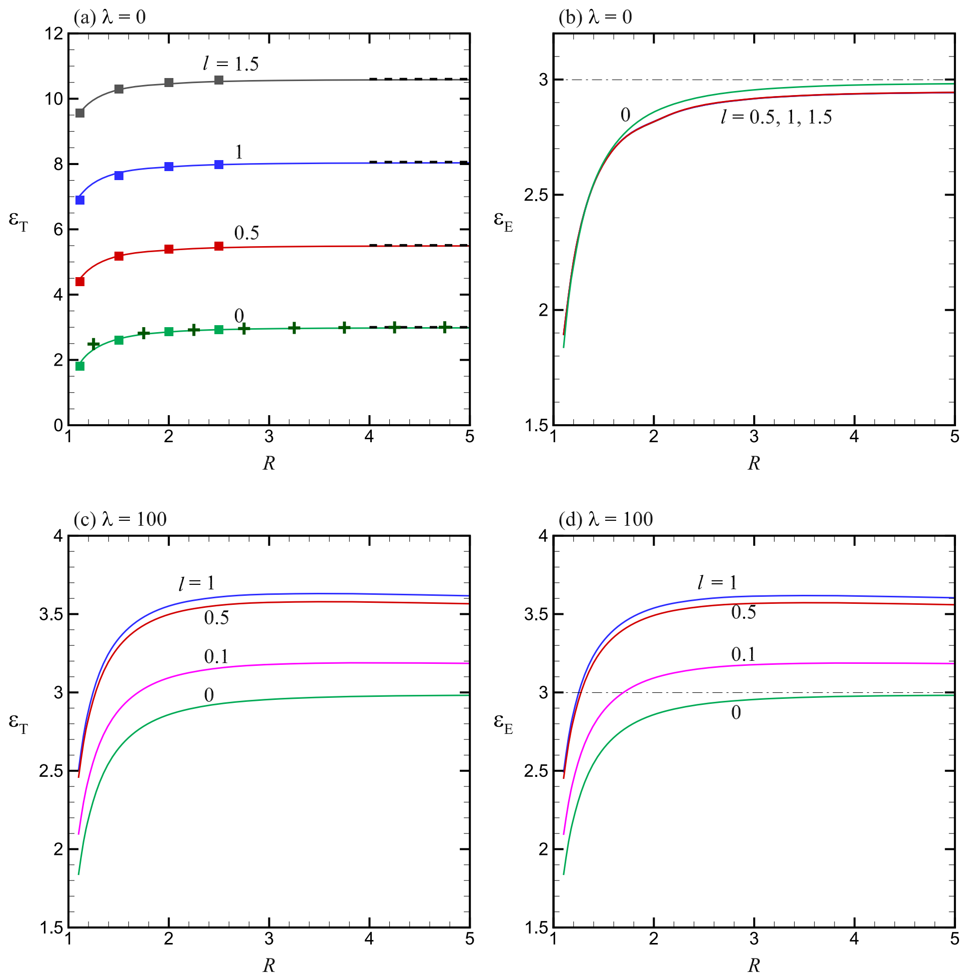

FIG. 3. The total flow resistance ε_T and the end resistance ε_E as functions of the proximity parameter R and length of the hole l, where the slip length $\lambda = 0$, 100. In (a), the squares are from the work of Wang,[9] the crosses are from the approximate formula Eq. (48) by Jensen *et al.*,[8] and the dashed lines are from the work of Dagan *et al.*[7] In (b), the values for $l = 0.5$, 1, 1.5 fall onto a single curve. In (b) and (d), the dashed-dotted line denotes the Sampson limiting value of 3.

Second, for $l > 0$, the end resistance can be much different from the value of 3 at $R \gg 1$, where the difference increases as l increases until l is larger than unity. In other words, under boundary slip, the channel length will have a more pronounced effect on the end resistance and the effect will persist until the channel is longer than order unity. Figure 3(d) provides an answer to the question that we have posed above. In the presence of boundary slip, the error of using the Sampson value of 3 to estimate the end resistance can be rather large and is on the under-estimate side. Our model generates the value of $\varepsilon_E = 3.61$ for $R = 5$, $l = 1$, and $\lambda = 100$. This amounts to some 20% larger than the Sampson value of 3. If Eq. (47) is used to estimate the total flow resistance, the resistance can be underestimated by 10%–17%, depending on the channel length and the slip length.

We further show in Fig. 4 how the total resistance ε_T and the end resistance ε_E may vary with the slip length λ, for $l = 0$, 0.1, 0.5, 1 and $R = 5$. Figure 4(b) reveals that, for $l > 0$, the end resistance may change non-monotonically with the slip length. Let us consider $l = 1$ as an example. When λ increases from 0,

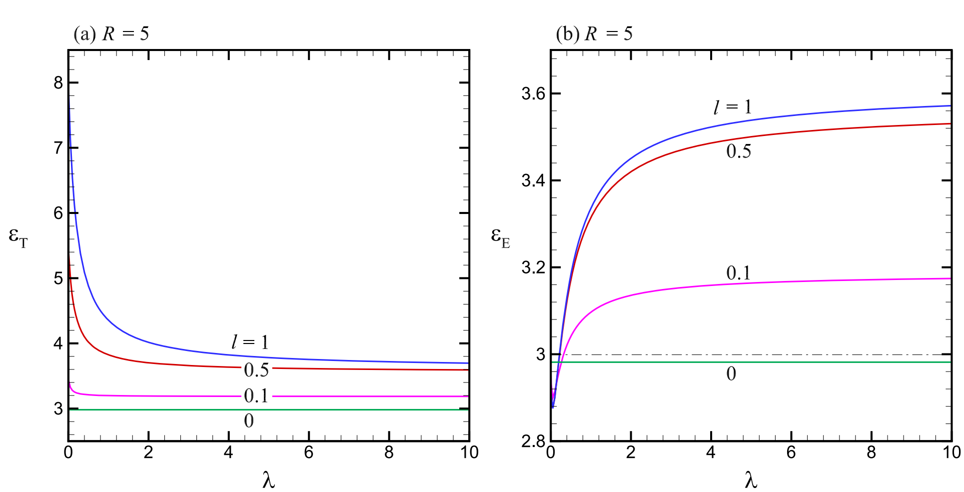

FIG. 4. The total flow resistance ε_T and the end resistance ε_E as functions of the slip length λ and length of the hole l, where the proximity parameter $R = 5$. In (b), the dashed-dotted line denotes the Sampson limiting value of 3.

ε_E will first decrease, reaching a minimum value of 2.88 at a very small $\lambda = 0.05$ and will then increase sharply in the range of $0.05 < \lambda < 1$. The increase in ε_E with λ becomes very mild as $\lambda > 5$. The figure clearly shows that, for any $l > 0$ and $\lambda > 0$, the end resistance is in general not close to the Sampson value of 3. Even for a modest slip length $\lambda \le O(1)$, the difference can be 10% or larger. Our findings point to the conclusion that Eq. (47) may not be a very good approximation formula to calculate the flow resistance of a slippery hole.

B. Entrance region

Apparently, the local pressure loss near the entrance to a channel is higher when the channel wall is slippery than when it is non-slippery. In order to understand this phenomenon, let us now look into some details about the flow in the vicinity of a channel inlet. In Fig. 5, we show the evolution of axial velocity profiles for two cases: (a) flow into a channel with no-slip wall and (b) flow into a channel with partial-slip wall of $\lambda = 10$. The values shown next to each profile denote the ratio of the velocity at the center or at the wall (for the slip case only) to that of the fully developed velocity profile. Some points are noteworthy. First, for $\lambda = 0$, the axial velocity profile at the inlet ($z_1 = 0$) is already very close to the fully developed parabolic velocity profile. The flow satisfies the no-slip boundary condition right at the inlet of the channel. Consequently, for the no-slip case, the entrance length is very short. A distance of 0.5 from the inlet is sufficient for the velocity to attain 99% of the ultimate profile. Only minor adjustment is needed as fluid particles traverse this entrance length. In sharp contrast, for $\lambda = 10$, the velocity profile will undergo a more dramatic change in the entrance region. Under the influence of wall slip, it takes a much longer distance for the velocity to attain its final profile. At the edge of the inlet ($r = 1$, $z_1 = 0$), the velocity is very small, which is dictated by the zero velocity on the barrier ($1 < r < 2$, $z_1 = 0$). Meanwhile, the velocity shear persists as fluid enters the channel. The velocity profile maintains a finite gradient near the wall at the inlet. In other words, the velocity profile does not satisfy the partial-slip condition right at the channel inlet. Major adjustment is needed immediately downstream from $z_1 = 0$. The velocity near the wall has to be increased, while the velocity gradient near the wall has to be decreased. During this course of development, a point of inflection shows up in the middle of the velocity profile. This is a point where the velocity gradient, and therefore the shear stress $\tau_{rz} = \partial w/\partial r$ (ignoring $\partial u/\partial z$), is maximum in magnitude. The occurrence of a maximum stress in the middle of a profile is easy to understand. The stress is always zero at the center ($r = 0$) and is nearly zero at the wall ($r = 1$) because of the slip condition. Therefore, for a non-uniform velocity profile, there should exist a point $0 < r_i < 1$ where the velocity gradient or the shear stress is maximum in magnitude.

The distribution of the velocity gradient, or shear stress, across the section will have a non-trivial effect on the pressure gradient. Using the notion of dominant balance, we may consider a balance between the axial pressure gradient and the radial diffusion of axial momentum,

$$\frac{\partial p}{\partial z} \sim \frac{\partial^2 w}{\partial r^2} \sim \frac{\partial \tau_{rz}}{\partial r}. \tag{49}$$

In a profile exhibiting a point of inflection at $r = r_i$, where the velocity gradient $\partial w/\partial r$ is maximum negative, the second

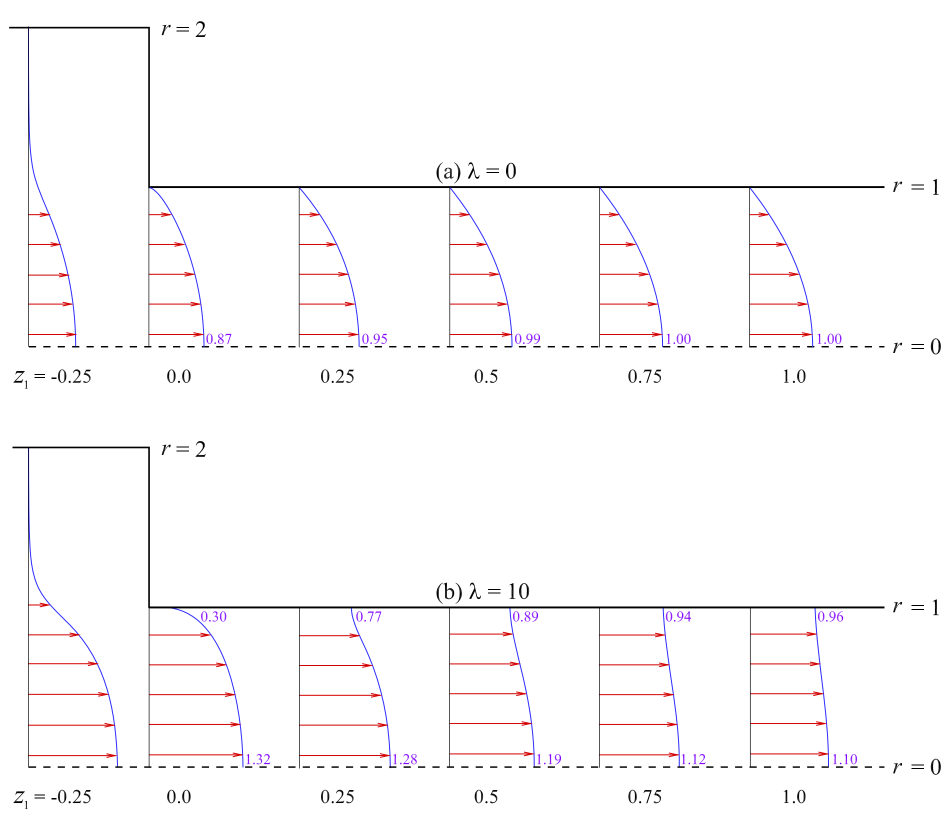

FIG. 5. Axial velocity profile $w(r)$ at various axial positions for (a) $\lambda = 0$ and (b) $\lambda = 10$, where $l = 1$ and $R = 2$. The values next to each profile are the velocity at the center and the velocity at the wall (slip case only) relative to those of the fully developed profile.

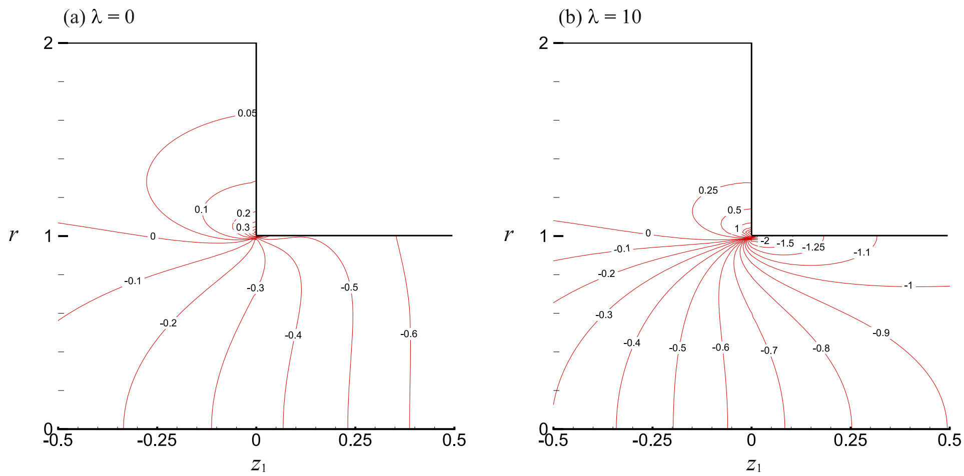

FIG. 6. Pressure fields $p(r, z_1)$ for (a) $\lambda = 0$ and (b) $\lambda = 10$, where $l = 1$ and $R = 2$.

derivative $\partial^2 w/\partial r^2$ is zero at $r = r_i$ and is negative and positive for $0 \le r < r_i$ and $r_i < r \le 1$, respectively. It follows from the above balance of dominant terms that the axial pressure gradient will change in sign across a section. The pressure gradient is negative (or favorable) near the center of the channel but is positive (or adverse) near the wall of the channel. At any cross section, there exists a point where the axial pressure gradient is zero.

The corresponding pressure fields are shown in Fig. 6. On comparing the two cases, one can find that the isobar patterns are similar in region I ($z_1 < 0$), but very different in region II ($z_1 > 0$). The pressure field shown in Fig. 6(a) resembles those presented previously by Dagan *et al.*[7] and Wang,[9] for flow near the entrance to a no-slip channel. There is a sudden change in pressure near the edge of the inlet, which is known to be a corner singularity in the pressure and stress fields. As remarked above, the entrance length in this no-slip case is very short. Also, a negative (favorable) pressure gradient prevails in the entrance region, and the loss is mainly to overcome wall friction.

For the partial-slip case, Fig. 6(b) shows a pressure field that echoes what we have discussed above. Here, we see a stronger corner singularity at the edge of the inlet. The pressure turns abruptly to a larger negative value around the corner. In the entrance region, the pressure gradient is indeed positive (adverse) near the wall but is negative (favorable) near the center. Here, the loss is not mainly to overcome wall friction but to overcome viscous stress located somewhere in the middle of the cross section. These aspects make the flow in the entrance region under the effect of slip fundamentally different from a fully developed Poiseuille flow. Similar findings have been reported by Ng and Sun[4] for flow through a channel where the wall changes abruptly from no-slip to partial-slip.

From what we have discussed so far, we can infer that the presence of boundary slip is to increase the departure of flow conditions (including kinematics and dynamics) at the channel inlet from those of the fully developed state. During the early stage of flow development, the fluid is in a state of shearing that is very different from that of the final state. As a result, a longer entrance length is required, and a more dramatic change in the pressure field is needed in order to develop flow in the entrance region. This explains why the end loss can be higher for flow through a slippery hole. The use of Sampson's formula may underestimate the end loss.

C. Empirical formulas

We have made an attempt to look for an empirical formula that can fit, as closely as possible, the results generated by our model for the end resistance as a function of l, R, and λ. We realize that it would be impossible to find a universally best-fit formula and many different functions can be used to do the fitting. Nevertheless, it is worth our effort if some simple formulas can be proposed. After some trials, we have come up with the following formulas:

$$\varepsilon_E = 1.53 + 1.42\left(1 - R^{-3.5}\right) + 0.62\tanh(3l)\tanh(0.8\lambda) \qquad \text{for } l = O(1), \tag{50}$$

$$\varepsilon_E = 3\left[1 - R^{-2.7}\right]^{0.33} \qquad \text{for } l = 0. \tag{51}$$

In Table I, we compare the results computed by these formulas (in brackets) with those generated by the model. For the cases shown in the table, the difference between the model and the formulas is not more than 2%. One is cautioned that these proposed formulas should only be used if quick calculations

TABLE I. Comparison of the end resistance ε_E, as computed by the model and the empirical formulas (50) and (51) (in brackets).

λ	R	$l = 0$	$l = 0.6$	$l = 0.8$	$l = 1$
0	2	2.858 (2.839)	2.817 (2.825)	2.818 (2.825)	2.818 (2.825)
	3	2.955 (2.948)	2.918 (2.920)	2.918 (2.920)	2.917 (2.920)
	4	2.976 (2.976)	2.938 (2.939)	2.938 (2.939)	2.937 (2.939)
	5	2.982 (2.987)	2.944 (2.945)	2.944 (2.945)	2.943 (2.945)
1	2		3.236 (3.214)	3.244 (3.230)	3.245 (3.234)
	3		3.331 (3.309)	3.340 (3.325)	3.342 (3.329)
	4		3.334 (3.329)	3.343 (3.344)	3.345 (3.349)
	5		3.333 (3.335)	3.342 (3.350)	3.344 (3.355)
10	2		3.481 (3.412)	3.498 (3.434)	3.503 (3.441)
	3		3.559 (3.507)	3.577 (3.530)	3.582 (3.537)
	4		3.562 (3.526)	3.579 (3.549)	3.583 (3.556)
	5		3.560 (3.532)	3.575 (3.555)	3.580 (3.562)

are needed, such as to find out how the end resistance is affected by the controlling parameters. For more accurate and reliable results, a full-blown model should always be used.

IV. CONCLUDING REMARKS

While Sampson's formula can be used with good accuracy to estimate the end loss incurred by Stokes flow through a no-slip pore of finite thickness, it does not work equally well when applied to flow through a slippery pore. The actual end resistance is larger than Sampson's value of 3 by 10% to 20% for moderate to large slip lengths. This is an error on the unsafe side when Sampson's value is inadvertently applied to, for example, flow through a frictionless nanochannel.[2,3] In this paper, we have examined how flow will adjust itself on entering a channel to attain the fully developed state. Without wall slip, little adjustment of flow is needed to bring flow at the inlet to the final state, resulting in a very short entrance region. In sharp contrast, the adjustment of flow in the entrance region is more dramatic under the effect of wall slip. The sudden change in the no-slip to partial-slip boundary condition will displace the point of maximum shear stress (also maximum vorticity) from the wall to somewhere in the middle of the cross section. This state of shearing will persist until the fully developed profile is attained. The flow is more rotational in the entrance region than in the fully developed region. This will entail greater energy loss in the entrance region, as energy is needed to maintain vorticity in this region.

ACKNOWLEDGMENTS

Financial support by the Research Grants Council of the Hong Kong Special Administrative Region, China, through General Research Fund Project No. 17206615 is gratefully acknowledged.

[1] M. E. Suk and N. R. Aluru, "Water transport through ultrathin graphene," J. Phys. Chem. Lett. **1**, 1590 (2010).
[2] T. B. Sisan and S. Lichter, "The end of nanochannels," Microfluid. Nanofluid. **11**, 787 (2011).
[3] C. Belin, L. Joly, and F. Detcheverry, "Optimal shape of entrances for a frictionless nanochannel," Phys. Rev. Fluids **1**, 054103 (2016).
[4] C.-O. Ng and R. Sun, "Pressure loss in channel flow resulting from a sudden change in boundary condition from no-slip to partial-slip," Phys. Fluids **29**, 103603 (2017).
[5] R. A. Sampson, "On Stokes's current function," Philos. Trans. R. Soc., A **182**, 449 (1891).
[6] H. L. Weissberg, "End correction for slow viscous flow through long tubes," Phys. Fluids **5**, 1033 (1962).
[7] Z. Dagan, S. Weinbaum, and R. Pfeffer, "An infinite-series solution for the creeping motion through an orifice of finite length," J. Fluid Mech. **115**, 505 (1982).
[8] K. H. Jensen, A. X. C. N. Valente, and H. A. Stone, "Flow rate through microfilters: Influence of the pore size distribution, hydrodynamic interactions, wall slip, and inertia," Phys. Fluids **26**, 052004 (2014).
[9] C. Y. Wang, "Stokes flow through a barrier with distributed pores," Chem. Eng. Commun. **197**, 1428 (2010).
[10] C.-O. Ng and C. Y. Wang, "Stokes flow through a periodically grooved tube," ASME J. Fluids Eng. **132**, 101204 (2010).
[11] J. Happel, "Viscous flow relative to arrays of cylinders," AIChE J. **5**, 174 (1959).
[12] R. Roscoe, "The flow of viscous fluids round plane obstacles," Philos. Mag. **40**, 338 (1949).